Proceedings of the Indian National Science Academy (2021) 87:613–627
https://doi.org/10.1007/s43538-021-00057-y

RESEARCH PAPER

Distribution of natural beta dose to individual grains in sediments

N. Chauhan[1] · T. P. Selvam[2] · S. Anand[2] · D. P. Shinde[1] · Y. S. Mayya[3] · J. K. Feathers[4] · A. K. Singhvi[1]

Received: 2 March 2021 / Accepted: 13 October 2021 / Published online: 21 October 2021

Abstract

In luminescence dating using single grains of quartz, statistical protocols are used to compute the most appropriate dose from the distribution of palaeodoses. The distribution of palaeodoses arises due to, (1) heterogeneity (at grain level) in bleaching at the time of deposition, (2) heterogeneous distribution of beta emitters present as randomly distributed feldspars (Mayya et al. in Radiat Meas 41:1032–1039, 2006) and, (3) heterogeneous distribution of grainsizes (Guérin et al. in Radiat Meas 47:778–785, 2015). Mayya et al. (Radiat Meas 41:1032–1039, 2006) demonstrated that random distribution of feldspar grains(with up to 14% stoichiometric K) and shorter range of beta particles (~ 2.3 mm in quartz) lead to significant variation in dose received by individual grains of quartz. This study improves upon Mayya et al. (Radiat Meas 41:1032–1039, 2006) by, (1) using a more realistic energy deposition function that was estimated using Monte Carlo simulations and (2) computing the effects of porosity of the sediment and beta straggling on the dose distribution function. It additionally concludes that effects of beta straggling are small and can be ignored. Ages based on new calculations led to improved concordance with control ages.

Keywords Luminescence dating · Quartz · Sediment beta dose · Monte Carlo simulations

Introduction

Over the last few decades, luminescence dating has emerged as a key tool to understand the chronology of recent earth surface processes. Luminescence dating provides the burial age of a sediment through the use of luminescence signal acquired by mineral grains constituting the sediment consequent to their exposure to ionizing radiations (α, β, γ and cosmic rays) arising from the decay of natural radioelements, viz. U, Th and K. The luminescence intensity of mineral grains is converted to radiation dose by using appropriate laboratory calibration experiments and is termed as palaeodose (D_e). Palaeodose when divided by annual dose (the dose rate), provides the age. The dose rate is computed using the measured concentrations of U, Th and K and standard conversion factors under the infinite matrix assumption, (Adamiec and Aitken 1998; Guérin et al. 2012).

More recent developments in instrumentation have enabled paleodose measurement using single grains, with the promise that the most bleached grains can be isolated and their signal be used for age analysis. Ideally, for a well behaved sample in which the luminescence signal is completely zeroed at time of deposition, the paleodoses estimated using individual grains of sediments are expected to be identical within the measurement errors. Thus, grains from same sediment stratum under a similar radioactive environment should give identical D_e values and the dose distribution should be a single valued delta $\delta(\overline{D})$ function around the mean dose. However, reports of considerable scatter in the single grain equivalent doses exist. Several workers have investigated the factors responsible for such distributions (Ankjærgaard and Murray 2007; Chauhan 2014; Chauhan and Singhvi 2011, 2019; Chauhan and Morthekai 2017; Cunningham et al. 2012; Guérin et al. 2015, 2012; Mayya et al. 2006; Murray and Roberts 1997; Nathan et al. 2003; Olley et al. 1998; Singhvi et al. 2011, 2010; Vandenberghe et al. 2003).

✉ N. Chauhan
naveenchauhan1983@gmail.com

1 Physical Research Laboratory, Ahmedabad 380 009, India

2 Health, Safety and Environment Group, Bhabha Atomic Research Centre, Mumbai 400 085, India

3 Indian Institute of Technology, Bombay, Mumbai, India

4 Department of Anthropology, University of Washington, Box 353100, Seattle, WA 98195-3100, USA

Beta heterogeneity: a review

Recent developments of luminescence dating have focussed towards understanding the nature and causes of distribution in palaeodoses (D_e) obtained for single grains or single aliquots comprising few hundred grains. Initially partial bleaching of sediments was considered to be the reason for distribution in the paleo-doses from grains (Chauhan 2014; Galbraith et al. 1999; Jain et al. 2004a, 2004b; Olley et al. 1999) but as the understanding about the dose distribution increased, other and possibly more important causes of the distribution in doses were identified. These included,

(i) partial zeroing of geological OSL prior to burial of the sediment (Olley et al. 1998, 1999),
(ii) heterogeneous distribution of beta doses that can be a significant fraction (generally ~ 30–60%) of the total dose, (Chauhan 2011; Guérin et al. 2015; Mayya et al. 2006),
(iii) variability in absorbed dose due to varied grain sizes (Guérin et al. 2015; Nathan et al. 2003),
(iv) bioturbation or pedoturbation (Bateman et al. 2007, 2003) and,
(v) unaccounted for sensitivity changes in luminescence response, during the measurement of paleodoses (Chauhan 2014; Chauhan and Singhvi 2011, 2019; Chauhan and Morthekai 2017; Singhvi et al. 2010, 2011)

Besides partial bleaching, heterogeneity in beta doses experienced by quartz grains at grain level, also leads to distribution in paleodoses (Mayya et al. 2006). Consequently significant inherent distribution in single grain and single aliquot doses occur due to beta heterogeneity. Heterogeneous beta dose deposition arises due to the range of beta particle being comparable to the grain size and the inter-grain distance. As a large fraction of beta dose in sediment matrix is contributed by randomly distributed K-Feldspar grains which act as hotspots, spatial fluctuations in the inter grain distances of feldspar hotspots from quartz grain results in a heterogenous deposition of beta dose.

Nathan et al. (2003) estimated the effect of heterogeneity of beta dose rate in sediments using Monte Carlo simulations and controlled laboratory measurements. They mimicked the heterogeneity of a natural sediment in respect of their radioactivity by using spheres of Al_2O_3:C and different materials of varied sizes mixed with pulverized radioacitive ore. High luminescence sensitivity of Al_2O_3:C, enabled measurement of the distribution of doses in Al_2O_3:C grains. A Monte Carlo radiation transport code was used to verify the experimental results and toextrapolate for other conditions in the field.

Nathan et al. (2003) demonstrated potential issues which can arise due to heterogeneous radiation environment in the nature, and its effect on D_e distributions. More specifically, they explored three aspects of heterogeneity of beta dose in nature viz.

(a) Estimation of the effect of attenuating bodies, packing density and atomic number on secondary electron flux and dose deposition.In this experimental realization heterogeneity of beta dosewas carried out and the results were compared with the Monte Carlo based simulations. Simulation experiments were not able to explain the experimental results fully. Experimental results gave higher relative standard deviation (RSD) as compared to Monte Carlo based results and, the variance in D_e increased with the heterogeneity.
(b) Numerical modeling to explore the effect of size of non radioactive material (clasts) on deposited dose. The simulations using variable size of calcium carbonate suggested that grains with higher diameters lead to higher spread in the D_e distribution.
(c) Models were tested for varying size of high radioactivity inclusions in the matrix. D_e distribution were significantly skewed and doses absorbed by grains were higher than Mean D_e.

Simulations by Nathan et al. (2003) did not accord with experimental results, but suggested that the heterogeneity in beta dose deposition is key to distribution in paleodoses. The study suggested that minor alteration in geometry can alter the D_e significantly and this leads to distribution in paleodoses. Further when the point sources of high radioactivity are heterogeneously distributed a tail in D_e distribution occurs which issimilar in shape, to the distribution arising from partial bleaching. Such situation may lead to erroneous interpretations and results.

Mayya et al. (2006) quantified the distribution of doses due to beta heterogeneity using an analytical model to estimate paleodose distribution in sediment matrix with unimodal grain size of 200 µm. Their model was based on a reasonable premise that in sediments, most of the β dose is contributed by a few K-feldspar grains (with up to 14% stoichiometric K) that are distributed randomly in a sediments matrix. Mayya et al. (2006) computed the heterogeneous deposition of beta dose resulting from random spatial fluctuation of K-Feldspar (hotspots) around individual quartz grains. As the mean range of β particle is comparable to inter grain distance and grain sizes, it implies that a feldspar grain near to a quartz grain deposits more dose in it as compared to the grains farther from it. Different quartz grains have different configurations of feldspar grains around them suggesting that the net dose delivered to them has an inherent distribution. Mayya et al. (2006) quantified spatial fluctuation of such β emitters in the sediment matrix and estimated the inherent distribution in the radiation doses to quartz grains. In this, the dose deposited by beta and gamma radiations arising from the decay of U, Th and secondary particles of cosmic rays was considered as spatially uniform and, only the beta dose from randomly distributed ^{40}K carrying feldspar mineral grains (hotspots) was taken as the sole cause for non-uniform dose deposition.

Heterogeneity in beta dose deposition was computed by examining the dose distribution in a quartz grain originating from fluctuations in the positions of K-feldspar (hotspots) grains and the range of beta particles. These computations suggested that spatial fluctuations resulted in positively skewed dose distribution curve and a modified age equation was therefore proposed to account for such a distribution of dose rates (Mayya et al. 2006). Mayya et al. (2006) computed this distribution in doses and demonstrated that this could be significant.

Cunningham et al. (2012) used a short lived ^{24}Na isotope to measure the nature of hetrogenous dose distribution along with Monte Carlo based MCNP4C simulations. The work used a sand box experiment in which quartz grains were mixed with artificially generated ^{24}NaOH spherical grains generated by bombarding NaOH with neutrons in nuclear reactor. The beta decay spectrum of ^{24}Na is similar to ^{40}K and thus was expected to provide similarresults. As the half life of ^{24}Na is ~ 14 h, it decaysand deposits its energy in nearby quartz matrix in laboratory time scale. The simulated distribution of beta doses and experimental distribution were positively skewed, but the dose spread from simulated results wereunderestimated, compared to the experimental results. The overdispersion (OD) of experimental data estimated solely due to beta hetrogeineity was 80%, while simulated data had an OD of 50%.The authors suggested that the packing fraction variation in model generated closed packing and natural packing could be a reason for this discrepancy.

Guérin et al. (2012, 2015) attempted amore realistic estimation of heterogeneity of beta dose deposition through Monte Carlo simulation using a GEANT-4 particle simulation code. They verified the results for a control age sand sample. They examined the distribution in the paleodose deposited in single grains of quartz by randomly distributed feldspar grains in a manner similar to the Mayya et al. (2006). However, instead of analytical formalism, a simulated sediment matrix of well sorted sand, with log normal distribution for fixed mean grain size was used. The simulations were similarly repeated for for several mean grain sizes. Radiation transport toolkit Geant4 was used for simulations. A random sediment matrix was generated considering a close packing fraction of 0.635 and the pore spaces were filled with water or air,which resulted in slightly different mean density of the matrix. The radiation sources (K feldspar hotspots) were considered to be randomly distributed through the matrix and the radioactivity within feldspar grains was considered to be distributed uniformly rather than a point source used by the Mayya et al. (2006). The paleodose distribution obtained was positively skewed as was suggested by Mayya et al. (2006), however the relative standard deviation was lower e.g. 20% (mean grain size ~ 255 µm) compared to 28% (constant 200 µm grain size). The authors attributed the discrepancies in observed values from two models to the assumptions made by Mayya et al. (2006). However, quantitive estimation of expected discrepancies between two methods was not provided as the two model approaches were different. The RSD increased with a decrease in K% content and/or increase in the mean grain size. The RSD was 135% for 0.14% K and for mean grain sizes of 635 µm. The RSD values estimated by Mayya et al. (2006) varied from 46 to 18% for K between 0.1 and 4%.

The scaled dose (defined as [dose]/[mean dose]) is an important parameter to estimate the minimum dose rate for estimating the ages. Although nothing much is mentioned about the minimum scaled doserates, but the data in the two papers suggest that they could be significantly different in two approaches as discussed above. The model (Guérin et al. 2015) explained the distribution in one sample and based on this, it was suggested that the age should be calculated using average dose and average dose rates without weighing the doses with their associated errors. Though debatable, this aspect is beyond the scope of present study. Though Guerin et al.'s, approach for simulating sample specific distribution gave good results, however its routine use may not be easy as sediments often have different grain size distribution and varied concentration of K (%). This calls for either of sample specific simulations or use (average dose)/(average dose rate) approach as suggested in their work.

Cunningham et al. (2012), further explored the effect of beta attenuation in variable grain size matrix. They suggested that mean dose rate to dosimeter grains depends on grain sizes distribution in the matrix. Based on Monte Carlo based simulations their results suggest that the attenuation of beta radiation for variable size of source grains, bulk sediments and dosimeter lead to significant differences in actual dose rate for dosimeters.

Using grain size dependent radioactivity measurements, it was suggested that U and Th are primarily present on the surfaces of grains and result in significantly higher dose rate than that predicted based on infinite matrix assumption. Further, for a well sorted grains it can be 9% to 14% higher. Cunnighnam et al. further suggested a balanced energy model which can overcome uncertainties due to the dose rate estimations and suggested to use tabulated values for beta attenuation factor for dose rate estimations. However as sediment matrices in nature would have varied grain size distributions, the use of tabulated attenuation coefficient values may be some what of an oversimplification of the problem.

The present study extended the analytical formulation of Mayya et al. (2006) by coupling these with the Monte Carlo based simulations for beta radiation dose deposition function determination. The quantification of beta dose distribution function was also refined, and a simple way to calculate ages as suggested by Mayya et al. (2006) was explored. The following sections discuss these refinements and their effects on dose distributions.

Distribution of beta dose at single grain level

In their initial study, Mayya et al. (2006) made several simplifications such as:

1. Approximations of specific energy loss (dE/dr) of beta particles by its mean value (E/R) where R is the range for an initial energy E.
2. Dependence of dose distribution on the packing density (porosity) of sediment matrix was not considered.
3. Variations due to straggling of beta rays were not considered.

The present study improves upon the calculation of dose deposition function, includes effect of porosity of soil and using a Monte Carlo simulation ascertains that the effects of straggling of beta rays is negligible (Fig. 1). Besides this, a computational error in Mayya et al. (2006), relating to the numerical evaluation of the integrals involving the range distribution function has been also rectified. Figure 1 gives a flow chart of methodology adopted for present computation and described in following section.

Dose deposited in a quartz grain in sediment

The quantity of concern is the dose (D_i) received by a quartz grain due to beta particles of all energies originating from an ith K-feldspar grain located at a radial distance (r_i). This was computed by estimating the energy deposited by a ^{40}K point source in quartz grain.

Figure 2 schematically shows a typical sediment matrix of average density ρ. The energy deposited by a ^{40}K β particle having energy with a range between R and $R+dR$ and located at a radial distance r_i from quartz grain is given by:

$$dE_i = p(R)dR \times \left(\frac{dE}{dr}\right)_{r=r_i} dr \times \frac{dA}{4\pi r_i^2} \tag{1}$$

here $p(R)dR$ is the range spectrum of ^{40}K β particles, dr is thickness of grain at r and dA is the cross-sectional area of

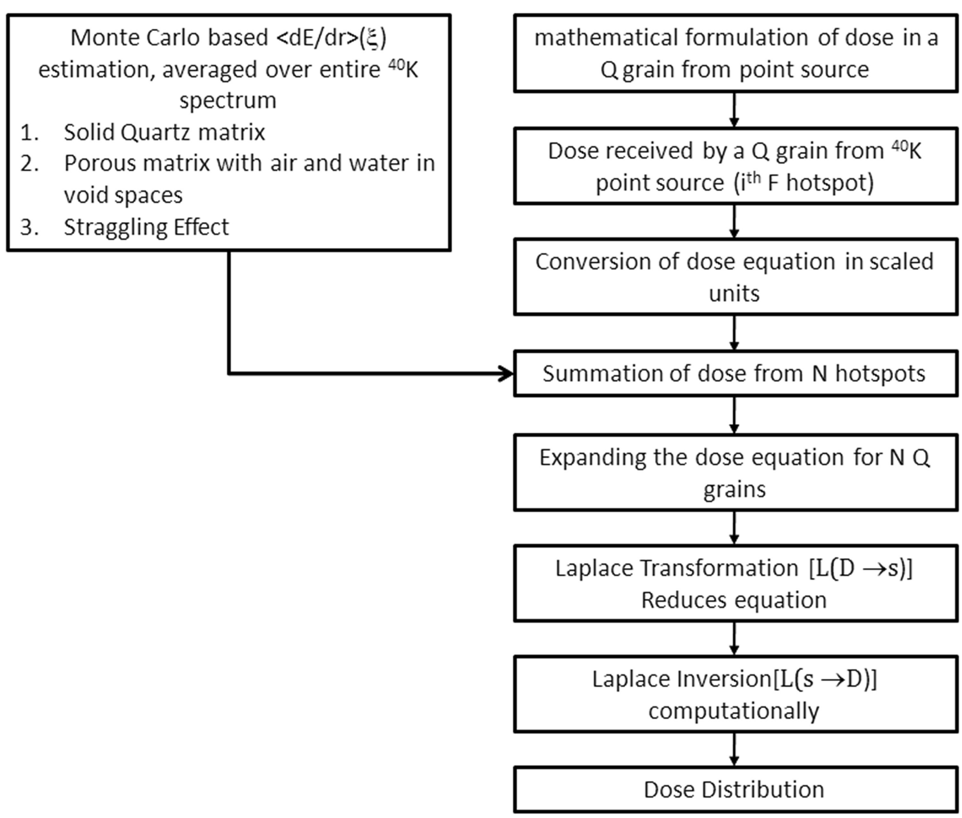

Fig. 1 Methodology adopted for computation of heterogeneous dose distribution using Monte Carlo simulations. Instead of analytical dE/dr, Monte Carlo based dE/dr is used at appropriate step

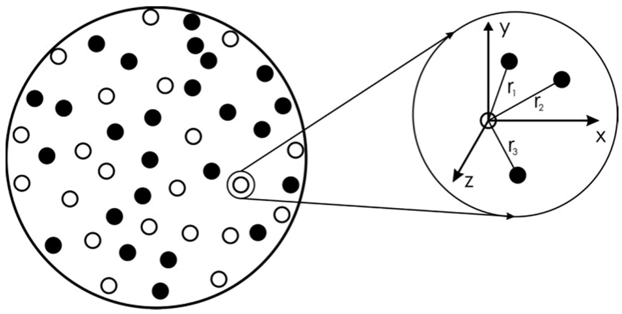

Fig. 2 Random distribution of quartz (white circles) and feldspar (black circles) grains in the sediment matrix resulting in heterogeneous dose deposition (Mayya et al. 2006)

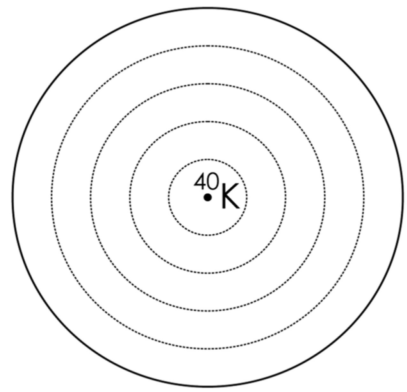

Fig. 3 The geometry used for the simulations. In this ^{40}K source at the center is surrounded by concentric spherical shells of quartz

the grain. The energy deposited by the complete ^{40}K spectrum with continuous energy in the region 0 to ~ 1.35 MeV is,

$$E_i = \int dE_i = \int_{r_i}^{R_m} p(R)dR \times \left(\frac{dE}{dr}\right)_{r=r_i} dr \times \frac{dA}{4\pi r_i^2} \tag{2}$$

where R_m is the maximum range corresponding to maximum energy E_m. The dose deposited in a grain of density ρ is given by dividing the above equation by $\rho dAdr$, the mass of the volume element $dAdr$.

Thus, the equation modifies to

$$D_i = \frac{1}{4\pi\rho r_i^2} \int_{r_i}^{R_m} p(R)dR \times \left(\frac{dE}{dr}\right)_{r=r_i} \tag{3}$$

The term inside the integral represents $\frac{dE}{dr}$ averaged over complete β range spectrum at a distance $r = r_i$

$$D_i = \frac{1}{4\pi\rho r_i^2} \langle \frac{dE}{dr} \rangle_{r=r_i} (\mathrm{r_i} < r < \mathrm{R_m}) \tag{4}$$

Equation (4) can be rewritten using dimensionless variables,

$$x = \frac{R}{R_m}, y(x) = \frac{E}{E_m}, \xi_i = \frac{r_i}{R_m} \tag{5}$$

as,

$$D_i = \frac{1}{4\pi\rho} \frac{1}{R_m^3} \left[\frac{1}{\xi_i^2} \langle \frac{dE}{dr} \rangle_{\xi=\xi_i} \right] (\xi_\mathrm{i} < \xi < 1) \tag{6}$$

where $\langle dE/dr \rangle_{\xi=\xi_i}$ is the energy deposition by a ^{40}K-feldspar hotspot, at a distance ξ_i. It can therefore be written as a function of ξ_i $\left(i.e.\langle dE/dr \rangle (\xi_i)\right)$ and can be calculated using Monte Carlo particle transport codes. Equation (6) can be further written as

$$D_i = D_c g\left(\xi_i\right) (\xi_\mathrm{i} < \xi < 1) \tag{7}$$

where D_c is the characteristic dose defined as

$$D_c = \frac{E_m}{4\pi R_m^3 \rho} \tag{8}$$

and g(ξ) is the dose-distance relationship function

$$g\left(\xi_i\right) = \frac{1}{\xi_\mathrm{i}^2} \left[\frac{\mathrm{R_m}}{\mathrm{E_m}} \langle \frac{\mathrm{dE}}{\mathrm{dr}} \rangle \left(\xi_\mathrm{i}\right) \right] (\xi_\mathrm{i} < \xi < 1) \tag{9}$$

where $\langle dE/dr \rangle \left(\xi_\mathrm{i}\right)$ is the energy deposition obtained by Monte Carlo simulation based particle transport codes. Finally, dose to a given grain due to all the hotspot are obtained by summing over all the K-feldspar sources as,

$$D = D_c \sum_{i=1}^{N} g\left(\xi_i\right) \tag{10}$$

Improvement in *dE*/*dr* using Monte Carlo simulations

While estimating the dose deposited by beta emitters averaged over their entire energy spectrum, Mayya et al. (2006) assumed dE/dr ~ E/R. This assumption was a first order approximation given that during the slowdown of β particles, the mass-collision-stopping power (MeV-cm^2/gm) increases, resulting in energy deposition at a higher rate. The earlier work by Guerin et al. (2015) gives the overall effect of the dose deposition function on dose distribution but does not provide dE/dr ~ r relation, explicitly. In the present study, the energy deposition by a β particle i.e. dE/dr was quantified using Monte Carlo simulations. The dE/dr function was estimated by Chauhan et al. (2009) and Chauhan (2011), and the same was used to compute the energy deposition with depth, with a higher resolution.

The geometry for simulations comprised a point ^{40}K source (Fig. 3) at origin surrounded by concentric spherical shells of thickness 10 µm. Spherical shells comprised quartz (SiO_2) of density 2.65 gm/cm^3. The beta energy spectrum of ^{40}K was taken from Kelly et al. (1959). A probability distribution curve for energy spectrum was generated by digitizing the data of ^{40}K spectrum from Kelly et al. (1959) and used for simulations in the form of a histogram with a bin width of ~ 66 keV.

Energy deposition by a β particle $\langle dE/dr\rangle$(r) is a function of distance between quartz and feldspar grain. This was quantified using Monte Carlo based EDKnrc user-code (Rogers et al. 2005) and EGSnrc code system (Kawrakow and Rogers 2000). These are software toolkits to perform Monte Carlo simulation of ionizing radiation transport through matter and, model the propagation of photons, electrons and positrons with kinetic energies between 1 keV and 10 GeV, in a homogeneous materials. This code utilizes Class-II condensed history Monte-Carlo techniques. The dataset on cross sections for the Monte-Carlo simulations was generated using PEGS4 program. This program creates material datasets for subsequent use by EGSnrc. Simulations were carried out to calculate the dose absorbed by a quartz grains at different radial distances for a point source (Fig. 3).Monte-Carlo simulations utilized the PRESTA-II electron-step-length algorithm and EXACT boundary-crossing algorithm (Kawrakow and Rogers 2000). ESTEP, the parameter that defines maximum fractional continuous energy loss per step was set to a default value of 0.25. In the simulations; the low energy threshold for electron transport was set to ECUT = 521 keV (i.e. 10 keV kinetic energy) and the photon transport cut-off parameter set to PCUT = 1 keV, after reaching these thresholds particle tracking is stopped. $\langle dE/dr\rangle$(r) was calculated for electron energies of 1.35, 1.25, 1.15, 1.05, 0.95, 0.85, 0.75, 0.65 MeV and was compared with the assumption $dE/dr \sim E/R$. Figure 4 shows one such comparison for 1.35 MeV and it is clear that its differs from a step function. Similar trends were observed for lower energies as well.

Using this, average specific energy loss, viz., $\langle dE/dr\rangle(\xi)$ was computed as a function of normalized distance. The normalization was w.r.t. the maximum range of ^{40}K beta particles. Variations for $R_m \times dE/dr(MeV)$ was obtained for the simulation results and compared with the computations of Mayya et al. (2006) in Fig. 5. This unit is used so as to compare similar terms on y axis. It shows that, at greater distances, the dose contribution by the ^{40}K hotspots is larger than that estimated by Mayya et al. (2006) i.e. quartz grains at larger distances receive upto 6–7% higher doses, as would be expected from the manner the dose

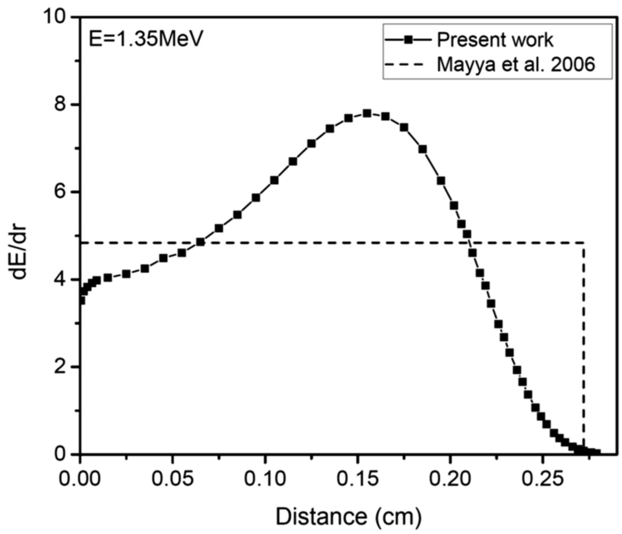

Fig. 4 The energy deposition function dE/dr as estimated by the Monte Carlo simulations compared with the function used by Mayya et al. (2006)

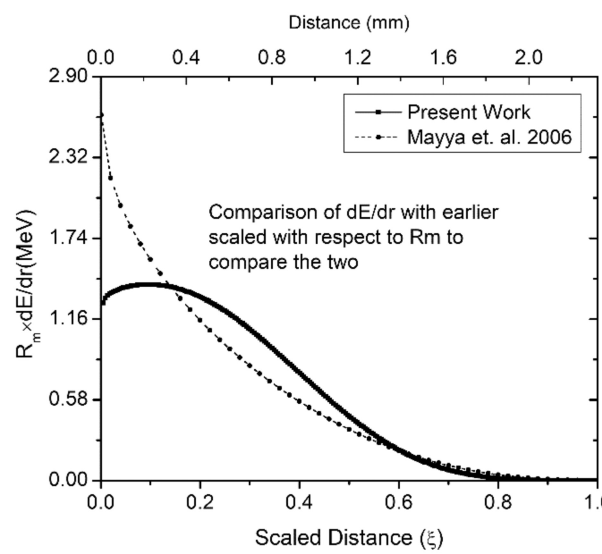

Fig. 5 The comparison of energy deposition function for the ^{40}K source obtained by Monte Carlo simulations with the Mayya et al. (2006). In this y axis is normalized in order to compare similar quantities on both sides

is deposited by beta as its energy is attenuated. Figure 6 shows the variation of energy deposited per unit volume $EPV = dose \times density$ as a function of scaled distance on a logarithmic scale. In this scale, both functions have almost similar shape; however, a disagreement of a few percent at scaled distance ξ ~ 0.3 occurs and reduces near ξ ~ 1. In

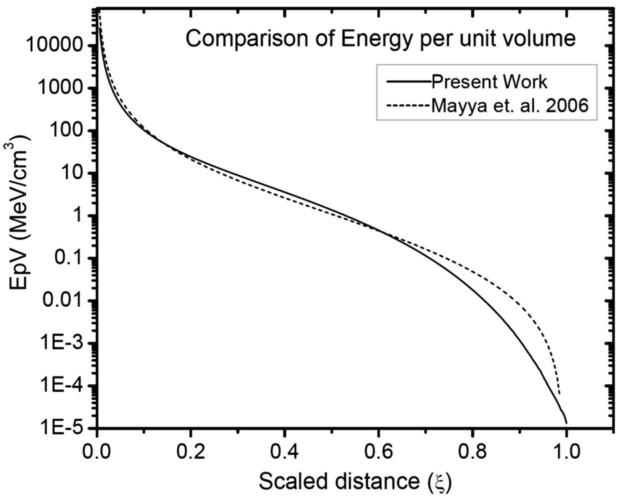

Fig. 6 Variation of energy deposited per unit volume (EPV) in different concentric shells of quartz by point source of ^{40}K. . The comparison with earlier work shows significant difference when scaled distance is ~ 0.3

the present calculations, the $\langle dE/dr\rangle(\xi)$ calculated using Monte Carlo simulation was used to compute the dose distribution in single grains, as discussed below.

Distribution of doses for single grains extracted from sediments

Equation (10) suggests that grains with the similar spatial configuration of feldspar grains around it will receive the same dose i.e. the dose distribution function $\phi(D)$ will be a δ function such that,

$$\phi(D) = \delta\left(D - D_c \sum_{i=1}^{N} g(\xi_i)\right) \tag{11}$$

The dose distribution function for different feldspar configurations was obtained using Mayya et al. (2006)'s approach and a Monte-Carlo generated function for $g(\xi_i)$. Equations (10) and (11) give the dose deposited and the corresponding distribution in dose of single grain of quartz from randomly distributed feldspar grains.

However as large number of such possible configurations exist; the actual distribution is the weighted sum of all these configurations taking into account their probability of occurrence. Thus, the Eq. (11) modifies to,

$$\phi(D) = \int_0^{\xi_m} \dots \int_0^{\xi_m} P(\xi_1, \xi_2 \dots \xi_N) d\xi_1 d\xi_2 \dots d\xi_N \times \delta\left(D - D_c \sum_{i=1}^{N} g(\xi_i)\right) \tag{12}$$

where $P(\xi_1, \xi_2 \dots \xi_N)$ is the net probability of occurrence of a configuration in which K-feldspar hotspots are at distances $\xi_1, \xi_2 \dots \xi_N$ from a given grain. Considering the concentration of K to be low (~ < 3%), the probability of occurrence of individual feldspar grains is independent of each other and hence the corresponding net probability density comprises a product of individual probability densities. Assuming that the individual probability of occurrence is uniformly distributed in space, the probability of occurrence of a feldspar grain in a small volume element in space is proportional to the ratio of the volume of the element and the accessible volume determined by the maximum beta particle range. In a dimensionless notation, this is,

$$P(\xi_i) d\xi_i = \frac{4\pi\xi_i^2 d\xi_i}{4\pi\xi_\infty^3/3} = \frac{3\xi_i^2}{\xi_\infty^3} d\xi_i \tag{13}$$

With these, Eq. (12) can be rewritten as

$$\phi(D) = \int_0^{\xi_m} \frac{3\xi_i^2}{\xi_\infty^3} d\xi_1 \dots \int_0^{\xi_m} \frac{3\xi_i^2}{\xi_\infty^3} d\xi_N \times \delta\left(D - D_c \sum_{i=1}^{N} g(\xi_i)\right) \tag{14}$$

Following Mayya et al. (2006), this N-fold integral was reduced further using Laplace transforms on the premise that dose being a positive quantity; its distribution should be zero for negative D. Thus as,

$$L[\phi(D)](s) = \int_0^{\infty} \phi(D) e^{-sD} dD \tag{15}$$

Laplace transformation from $D \to s$ decomposes the N-fold integral to the Nth power of a single integral which is easier to solve numerically. Thus expressing the dose distribution function in terms of scaled dose units as $\phi\left(D/\overline{D}\right)$, its Laplace transform $\phi^*(s)$ satisfies the equation,

$$\phi^*(s) = e^{\mu[f(s)-1]} \tag{16}$$

where μ is the mean number of hotspots ($\mu = 892 \times k$, where k is % of K and 892 arises from the total number of grains per %K per cc) within the maximum range R_m and the function $f(s)$is related to the dose-distance function g(ξ) through the relationship,

$$f(s) = 3\int_0^1 \xi^2 e^{-sg(\xi)} d\xi \tag{17}$$

The final dose distribution is obtained using the Laplace inversion ($s \to D$) of the function on the RHS of Eq. (16). Numerical inversion programme of Mayya et al. (2006) was used for inversion. Function $f(s)$ defined in Eq. (17) was evaluated using function g(ξ) (Eq. (9)) and $\langle dE/dr\rangle(\xi_i)$ values estimated using Monte Carlo simulation of electron/photon transport. For evaluating the integral, the $\langle dE/dr\rangle(\xi_i)$ values were fitted to a polynomial function, viz.,

$$\begin{aligned} p(r) =& 5.21765 + 7.34693r - 28.05728r^2 - 76.6174r^3 \\ &+ 244.60605r^4 - 214.6201r^5 + 62.10964r^6 \end{aligned} \tag{18}$$

Laplace inversion of $\phi^*(s)$ yields the required dose distribution $\phi\left(D/\overline{D}\right)$ for different concentrations of K (Fig. 7).

Figure 7 shows a comparison of the dose distribution function with that from Mayya et al. (2006). The dose distribution peak is shifted to higher doses by 25% to 13% for K concentrations varying from 0.3 to 3% respectively. This occurs due to higher energy deposition by sources situated at larger distances (~ 0.4–1.5 mm) (Fig. 5) as compared to the estimates using the mean energy approach (Fig. 7). This is possibly due to increased LET when the beta particles slow down towards the end of their range and this leads to higher energy deposition. The volume of the spherical shell between 0.4 and 1.5 mm is larger compared to the volume for sphere (r < 0.4 mm) where energy deposition is higher as suggested by mean energy approach. This also implies that number of feldspar grains is comparatively larger (due to larger volume) than the proximal ones (whose contribution is estimated to be smaller than mean energy approach) and on the whole, a higher dose is deposited in the quartz grains. The shift in the dose distribution function towards higher dose changes the minimum dose rate to a higher value and thereby would correspondingly lead to lower age as compared to Mayya et al. (2006).

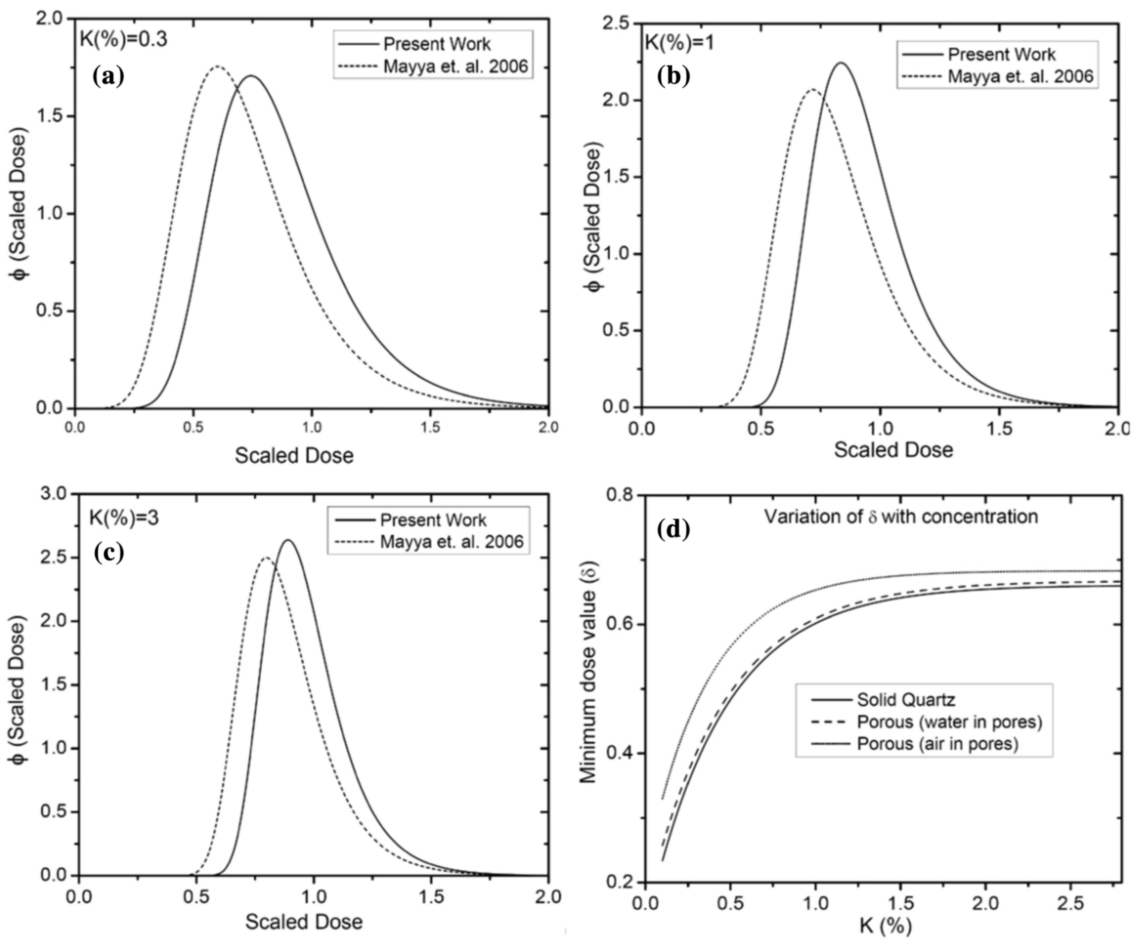

Fig. 7 **a–c** The dose distribution function $\phi\left(D/\overline{D}\right)$ obtained using Monte Carlo simulations for different concentrations of the K. There is systematic shift of the distribution function towards higher dose side as compared to Mayya et al. (2006). **d** Variation of minimum-scaled dose (δ) with concentration of K for variable porosity

Porosity and water content

The dose distribution for a homogeneous, quartz medium was then modified to account for the porosity and moisture content. To realize the natural conditions, a porosity of 30% was incorporated in the Monte Carlo simulations by using a geometry that comprised alternate spherical shell of quartz and air (Fig. 8). The thickness of the air shell was considered such that the volume of the shell equals porosity times the volume of the inner quartz shell $\left(Volume_{air} = Porosity \times Volume_{quartz}\right)$. Similar simulations were carried out for dose distribution when all the air shells were filled with water. Dose deposition functions for these calculations are shown in Fig. 9a–c. As expected, effective range of the β particle is higher for higher porosity and is lower for higher moisture content.

The dose distribution function for a porous sediment matrix is given as *ϕ(Scaled dose) vs. Scaled dose* plot in Fig. 9a–c. It shifts towards higher dose as compared to solid quartz. The dose distribution function when the pore spaces are filled with water '*Porous (water in pores)*'(*ϕ(Scaled dose) vs. Scaled dose* plot in Fig. 9a–c; lies in between these two extremes, but nearly overlaps with the distribution for solid quartz. Further, the relative shift decreases as concentration of potassium increases. Any shift in the dose distribution function is due to the increase in the range of β particles in porous and moist sediments relative to solid quartz.

As the effective volume (within the R_{max}) contributing to the beta dose increases, the average dose deposited in a particular grain increases. An increase in deposited dose shifts the dose distribution function to higher side. As the potassium content increases, the relative shift decreases due to decrease in heterogeneity with increase in concentration.

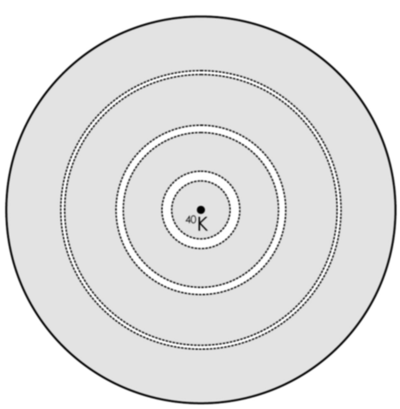

Fig. 8 The geometry used in simulation to incorporate the effect porosity and study the effect of water content on dose distribution function

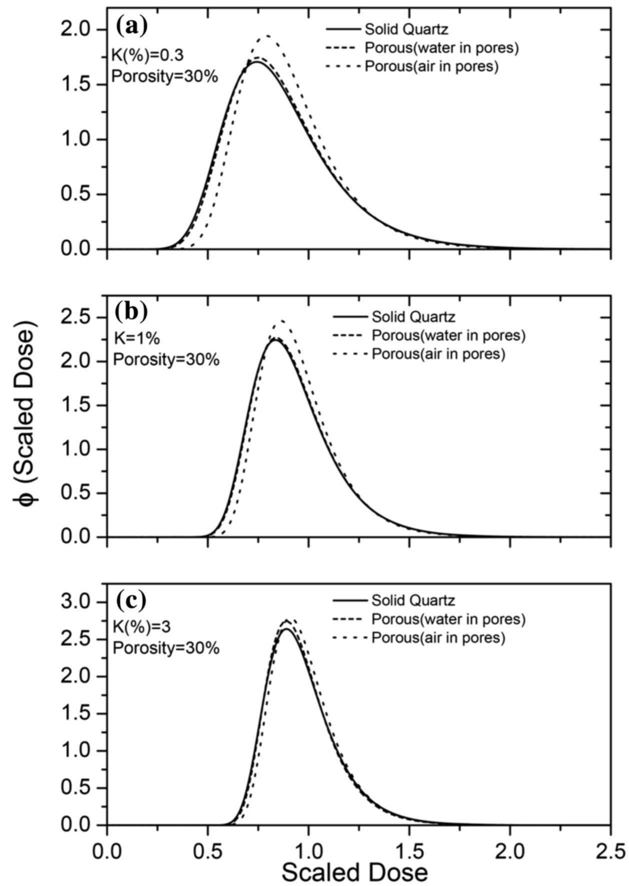

Fig. 9 Dose distribution function $\phi\left(D/\overline{D}\right)$ computed for sediment matrix having 30% porosity for different concentrations of K

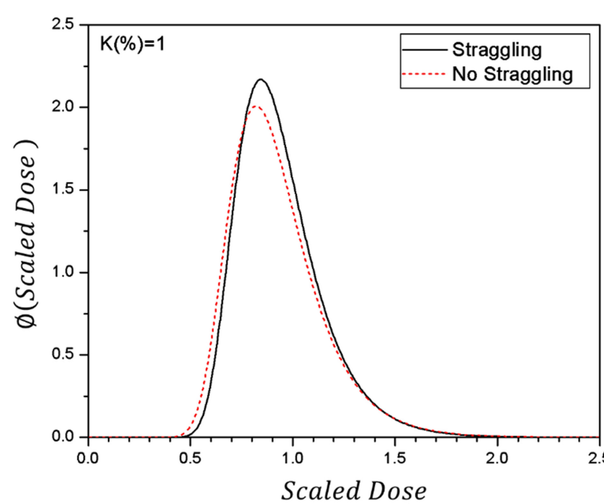

Fig. 10 Effect of straggling on dose deposition function

In addition to this, the effect of beta range straggling was also considered, however changes in dose distribution were negligible (Fig. 10) and hence were not explored further and are not therefore discussed further.

Implications: single grain dose distribution

Figure 7a–c show a shift in the dose distribution function towards the higher dose values, when the approximation dE/dr ~ E/R is improved upon by a more realistic function. An increase in the minimum-scaled dose (δ) occurs. The shift in distribution affects the age depending on the fraction of uniform and non-uniform doses as in Eq. (19) by Mayya et al. (2006),

$$T = \frac{D_{min}}{[f + \delta(1 - f)]\overline{\dot{D}}} \tag{19}$$

In this equation T is the age, D_{min} is the minimum D_e of experimentally observed values, *f* is the fraction of uniform dose rate calculated as fraction of total dose-rate by, (i) beta radiation from U and Th, (ii) gamma radiations from U, Th and K and, (iii) cosmic rays (CR).

Here, $\overline{\dot{D}}$ is the average dose rate of the sediments,δ is the value of the minimum scaled dose up to which probability of distribution $\phi(D)$ is 10% and is read from the dose distribution functions for a given K value (Fig. 7). The value of 10% is chosen as the minimum values of dose distribution are often subject to fluctuations. As δ corresponds to a 10% probability so, D_{min} in the present cases also correspond to the 10% probability. The procedure for its estimation is described in following section. The δ values increases with increasing concentration of potassium and saturates at higher concentrations, (Fig. 7d for different K concentrations). The value of δ at a given concentration is calculated using the following empirical relation obtained by fitting the asymptotic curve (Fig. 7d) to δ values for different concentrations,

$$\delta = 0.66 - 0.53(0.11)^{x} \tag{20}$$

where x is the K (%).

Typically δ increases from 0.23 (for x = 0.1) to a maximum value of 0.66 (for x ~ 3 or more). Thereafter any further increase in concentration of K leads to an increase in peak height and a decrease in Full Width Half Maximum (FWHM). This is expected as the effect of spatial fluctuations weakens with increase in K concentration and the distribution approaches aδ distribution around an average dose ($\overline{D}$).

Porosity influences the δ value. Figure 7d provides the variation of doses with the porosity of the sediment matrix for different concentrations of K. For a given concentration of K, the δ increases with a decrease in density of the matrix. δ is higher for a porous soil in which voids are filled with air, while for the moist soil, it lies in between the two extreme cases i.e. solid and voids filled with air.

For moist conditions the graph for '*Porous (water in pores)*' gives more realistic results, while for dry samples '*Porous (air in pores)*' is appropriate. The values of δ for different concentration can be obtained from following empirical relations.

For dry soil, '*Porous (air in pores)*'

$$\delta = 0.68 - 0.46(0.06)^{x} \tag{21}$$

For Moist soil, '*Porous (water in pores) 30% porosity*'

$$\delta = 0.68 - 0.51(0.11)^{x} \tag{22}$$

Here *x* is the K (%). As the concentration increases, the relative shift in the distribution functions for different densities decreases.

Experimental validation of computational results

To test the results from this study, single grain age results from the Southern High Plains (Feathers 2003; Feathers et al. 2006a) and the Cactus Hill Site (Feathers et al.

Table 1 Methodology to obtain age using beta heterogeneity concept of present study

S. no.	Steps
1	Obtain dose distribution
2	Compute minimum dose (D_{min}) using 10% probability model
3	Compute average dose rate $\left(\overline{\dot{D}}\right)$
4	Estimate fraction of uniform dose, $f = \left(\dot{D}_{\gamma}(U, Th, K) + \dot{D}_{\beta}(U, Th)\right)/\overline{\dot{D}}$
5	Compute δ value using Eqs. (20), (21) and (22)
6	Estimate age using Eq. (19), $T = \frac{D_{min}}{[f+\delta(1-f)]\overline{\dot{D}}}$

Here, $\overline{\dot{D}}$: average Dose rate,, f: fraction of uniform dose, $\dot{D}_{\gamma}$: gamma dose rate, $\dot{D}_{\beta}$: beta dose rate, D_{min}: minimum dose, T: age, δ: minimum scaled dose

Table 2 The results were tested for 24 samples from, Southern Hill Plains (Feathers 2003; Feathers et al. 2006a) and Cactus Hill Site (Feathers et al. 2006b) dated earlier independently by single grain luminescence and also had independent age control

Samples	Total DR (uGy/a)	K (%)	K-40 β DR (uGy/a)	δ	f	Minimum DR (Gy/ka)
Southern High Plains (Feathers et al. 2006a)						
uw479	1601 ± 99	0.61 ± 0.01	414	0.60	0.74	1.43 ± 0.09
uw480	1916 ± 158	1.00 ± 0.02	607	0.65	0.68	1.71 ± 0.14
uw568	1916 ± 143	0.92 ± 0.01	629	0.65	0.67	1.69 ± 0.13
uw569	2719 ± 206	1.52 ± 0.04	1004	0.67	0.63	2.39 ± 0.18
uw570	2821 ± 151	1.43 ± 0.02	983	0.67	0.65	2.50 ± 0.13
uw571	1766 ± 146	0.71 ± 0.02	448	0.62	0.75	1.59 ± 0.13
uw573	1905 ± 164	0.78 ± 0.03	522	0.63	0.73	1.71 ± 0.15
uw575	927 ± 51	0.44 ± 0.01	311	0.55	0.66	0.79 ± 0.04
uw579	3144 ± 182	1.52 ± 0.01	1046	0.67	0.67	2.80 ± 0.16
uw580	2797 ± 211	1.35 ± 0.03	883	0.67	0.68	2.51 ± 0.19
uw582	1927 ± 280	1.15 ± 0.08	601	0.66	0.69	1.72 ± 0.25
uw585	701 ± 46	0.18 ± 0.01	127	0.40	0.82	0.63 ± 0.04
uw586	582 ± 44	0.14 ± 0.01	99	0.37	0.83	0.52 ± 0.04
uw587	451 ± 33	0.10 ± 0.01	71	0.33	0.84	0.40 ± 0.03
Cactus Hill Site (Feathers et al. 2006b)						
uw435	2618 ± 106	2.03 ± 0.02	1422	0.68	0.46	2.16 ± 0.09
uw436	2421 ± 110	1.86 ± 0.06	1303	0.68	0.46	2.00 ± 0.09
uw438	2393 ± 184	2.01 ± 0.18	1356	0.68	0.43	1.96 ± 0.15
uw617	2534 ± 131	2.02 ± 0.06	1409	0.68	0.44	2.08 ± 0.11
uw618	2604 ± 124	2.08 ± 0.01	1451	0.68	0.44	2.14 ± 0.10
uw696	2637 ± 105	2.08 ± 0.01	1478	0.68	0.44	2.16 ± 0.09
uw697	2842 ± 176	1.99 ± 0.13	1438	0.68	0.49	2.38 ± 0.15
uw698	2549 ± 103	1.97 ± 0.02	1383	0.68	0.46	2.10 ± 0.09
uw700	2414 ± 103	1.95 ± 0.03	1328	0.68	0.45	1.99 ± 0.08
uw701	2509 ± 104	2.01 ± 0.01	1369	0.68	0.45	2.07 ± 0.09

The table gives calculated values of minimum scaled doses (δ) and fractions of uniform doses (f) for the samples used in the study. Courtesy: James K. Feathers

DR dose rate

Note: Some of the samples were not used due to unresolved inconsistencies in the dose rates

2006b) were used. Samples from the Southern High Plains had independent and secured radiocarbon ages. Ages from Cactus Hill Site had an age control based on archaeological information. Table 1 gives the methodology for computation of ages using present study. The δ values were computed for a given K% and the fractions of uniform (f) and non-uniform dose (1 − f) were estimated from radioactivity concentration of U, Th, K and cosmic rays (Table 2). Minimum dose rates were computed from values of δ, f and average dose rates ($\bar{D}$).Ages were estimated by two approaches using the data from Southern High Plains (Feathers 2003; Feathers et al. 2006a) and Cactus Hill Site (Feathers et al. 2006b).

1. In the first approach, palaeodoses having error > 20% were not considered and the remaining doses were arranged in increasing order. The palaeodose values where 10% probability criterion is fulfilled were identified, i.e., the N^{th} dose value, such that N = 10% of number of dose values. The age was then calculated using estimated dose and minimum dose rate (Eq. (19)).
2. In second method the minimum age model (MAM) doses estimated by Feathers et al. (2006a, b); were used for estimating ages using Eq. (19) (Table 1).In the published works for Southern High Plains, the minimum ages were calculated using an input over-dispersion parameter of 0.18 based on the highest over-dispersion calculated in dose recovery for individual samples.

While for Cactus Hill, no input over-dispersion parameter used in determining the minimum age. However, a simple test for one of the samples UW699, it was found that it does not make much of a difference in this case because of the relatively high uncertainties in the D_e estimation of each grain. For example, for UW699, the original MAM value is 47 Gy. Redoing with a 0.1 sigma-b, the value becomes 48 Gy, which is well within the uncertainties of the original estimation.

Figure 11 and Table 3 compares the estimated ages with the published and control ages. The ages estimated by the two methods agree with published and control ages. For 24 samples, 22 ages are in accordance with expected control ages and/or give better approximation of expected ages than age results based on conventional approach.

Two samples UW585 and UW586 underestimate the age. Samples UW585 and UW586 were from an eolian sand in Southern High Plains with low K (< 0.18%) overlain by clay rich lamellae and loamy sand on top. We consider that in these cases, K is most likely also present in finer grains and these are distributed uniformly leading to a uniform dose. In such cases the beta dose distribution will change and ages using minimum dose will be underestimated.

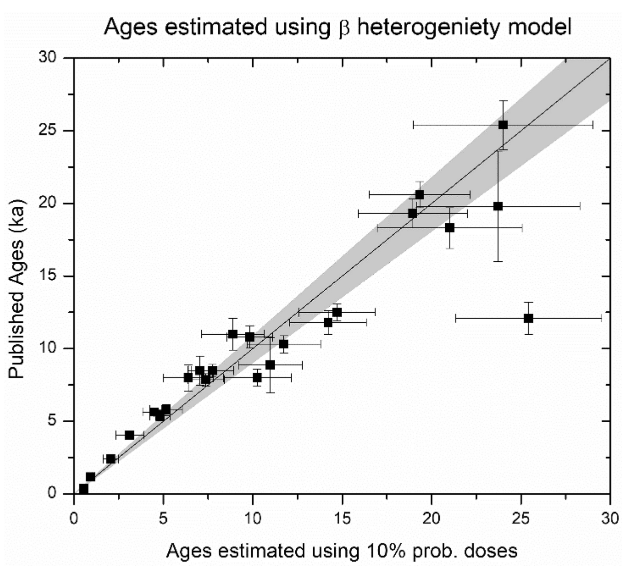

Fig. 11 Comparison of published ages (Feathers 2003; Feathers et al. 2006a; Feathers et al. 2006b) with present ages. The ages are consistent with published ages and also found to be in agreement with control ages (Table 2). The shaded region shows 10% probability band for 1:1 line

Discussion

The present work refines the dose distribution derived by Mayya et al. (2006) by computing the dose-depth profile using Monte Carlo simulations and corrects a computational error. These two changes resulted in a shift in the peak of dose distribution function (25% to 13% for K (%) = 0.3 to 3 respectively). This shift in dose distribution function translates to higher beta doserate compared to Mayya et al. (2006). Another important factor which is linked to distribution in single grain doses is relative standard deviation (RSD). Present work suggests that the RSD of dose distribution obtained in present work is universally lower than that obtained by Mayya et al. (2006). The RSD for K concentrations of 0.3%, 1% and 3% were 32%, 23% and 18% respectively in comparison to 37%, 28% and 21% obtained by Mayya et al. (2006). Although it is not appropriate to compare the obtained RSD with Guérin et al. (2015) as that work uses log normal distribution of grain size instead of single grain size which is used in present study but an approximate comparison can be made. The RSD obtained by Guérin et al. (2015) for 1% K for a mean grain size of 255 μm is 20% which is similar to value obtained in present work but lower than Mayya et al. (2006). Guérin et al. (2015) attributed this discrepancy to difference in approach used in the two methods and differences in parameters used in the modelling and possibly straggling.

The present work clearly brings out that straggling plays minimal role which is also suggested by simulation of Guérin et al. (2015). Cunningham et al. (2012)'s simulation of the beta heterogeneity of natural ^{40}K by using fast decaying artificial ^{24}Na beta emitting source, gave a positively skewed distribution similar to present work and those by Mayya et al. (2006) and Guérin et al. (2015). The over dispersion observed by Cunningham et al. (2012) in single grain doses of quartz mixed with ^{24}NaOH in sand box experiment was about 82% while in case of gamma dosed quartz it was ~ 17%, which enabled them to suggest that high OD (quadrature subtraction ~ 80%)was due to effect of heterogeneous beta dose deposition. Further Monte Carlo simulations simulating same sandbox model resulted in an OD of 50% which was less than the observed values. However, these values are difficult to compare against estimated RSD values as it is difficult to know the sources of scatter contributing in their experiments.

In addition, the work further enables a more realistic approximation to natural environment as it includes the effect of the porosity and water content. The effect of porosity was introduced by means of alternate concentric spherical shells of air/water and quartz. Till now, the effect of porosity during simulations was introduced by considering uniform average density instead of shells like geometry.

Table 3 The table compares the computed ages with published ages and independent control ages for 24 samples from, Southern Hill Plains (Feathers 2003; Feathers et al. 2006a) and Cactus Hill Site (Feathers et al. 2006b) dated earlier independently by single grain luminescence and also had independent age control

Samples	Doses		Ages			
	MAM Dose (Gy)	10% Prob. Dose (Gy)	MAM Age (ka)	10% Prob. (ka)	Published ages (ka)	Expected age (ka)
Southern High Plains (Feathers et al. 2006a)						
uw479	9.0 ± 0.6	7.4 ± 1.2	6.3 ± 0.6	5.2 ± 0.9	5.81 ± 0.33	5.8 (14C)
uw480	14.8 ± 1.1	13.2 ± 1.7	8.7 ± 0.9	7.7 ± 1.2	8.48 ± 0.44	9.45 (14C)
uw568	0.8 ± 0.04	0.9 ± 0.1	0.5 ± 0.04	0.5 ± 0.1	0.37 ± 0.14	0.5 (14C)
uw569	6.5 ± 0.4	4.9 ± 1.0	2.7 ± 0.3	2.1 ± 0.4	2.41 ± 0.13	2.0 (14C)
uw570	11.4 ± 0.8	11.2 ± 1.5	4.5 ± 0.4	4.5 ± 0.6	5.64 ± 0.25	5.65 (14C)
uw571	14.2 ± 0.5	11.8 ± 1.3	8.9 ± 0.8	7.4 ± 1.0	7.86 ± 0.42	8.6 (14C)
uw573	10.2 ± 0.5	8.2 ± 0.6	6.0 ± 0.6	4.8 ± 0.6	5.37 ± 0.34	1.3 (14C)
uw575	9.1 ± 0.9	7.7 ± 0.9	11.6 ± 1.3	9.8 ± 1.3	10.8 ± 0.77	11.5 (Plainview points)
uw579	1.8 ± 0.5	2.6 ± 0.5	0.6 ± 0.2	0.9 ± 0.2	1.16 ± 0.17	< 1.7 (14C)
uw580	25.9 ± 2.7	27.5 ± 4.0	10.4 ± 1.3	11.0 ± 1.8	8.87 ± 1.9	< 9–13.5 (14C)
uw582	7.0 ± 0.7	5.4 ± 1.1	4.1 ± 0.7	3.1 ± 0.8	4.04 ± 0.31	> 2.0 (14C)
uw585	5.7 ± 0.8	5.6 ± 1.0	9.1 ± 1.4	8.9 ± 1.8	11.0 ± 1.1	12.7 (Folsom Points)
uw586	3.4 ± 0.5	3.3 ± 0.7	6.6 ± 1.1	6.4 ± 1.4	7.99 ± 0.89	11.1 (Firstview Points)
uw587	2.8 ± 0.4	2.8 ± 0.2	6.8 ± 1.1	7.1 ± 0.7	8.48 ± 1.0	2.0 (14C)
Cactus Hill Site (Feathers et al. 2006b)						
uw435	21.1 ± 1.4	22.2 ± 4.0	9.8 ± 0.8	10.3 ± 1.9	8.0 ± 0.6	10
uw436	24.9 ± 1.1	23.5 ± 4.0	12.4 ± 0.8	11.7 ± 2.0	10.3 ± 0.6	10
uw438	51.7 ± 4.3	47.0 ± 9.1	26.4 ± 3.0	24.0 ± 5.0	25.4 ± 1.7	23.5
uw617	42.8 ± 3.1	39.4 ± 6.0	20.6 ± 1.8	18.9 ± 3.1	19.3 ± 1.0	> 18
uw618	41.1 ± 6.8	41.3 ± 5.7	19.2 ± 3.3	19.3 ± 2.8	20.6 ± 0.9	> 20
uw696	31.4 ± 2.8	55.0 ± 8.5	14.5 ± 1.4	25.4 ± 4.1	12.1 ± 1.1	22.5
uw697	32.4 ± 1.3	33.8 ± 4.6	13.6 ± 1.0	14.2 ± 2.1	11.8 ± 0.8	15
uw698	31.4 ± 1.2	31.0 ± 4.3	14.9 ± 0.8	14.7 ± 2.1	12.5 ± 0.6	15
uw700	48.1 ± 9.1	47.1 ± 8.9	24.2 ± 4.7	23.7 ± 4.6	19.8 ± 3.8	> 21
uw701	46.1 ± 3.2	43.5 ± 8.2	22.3 ± 1.8	21.0 ± 4.1	18.3 ± 1.4	> 22

MAM minimum age model. Courtesy: James K. Feathers

However, in such an approach although the depth dose relationship is included but the energy absorbed by water/air is not accounted. As said above, this study also suggests that the effects due to beta straggling are small and can be neglected.

We also suggest the use of a simple procedure to calculate the ages Eq. (19), given by Mayya et al. (2006). This is based on estimation of age based on minimum dose and minimum dose rate value and relies on a reasonable consideration that minimum palaeodose will accrue from (i) most bleached grains, (ii) least dosed grains.

Guérin et al. (2015) however suggest to use arthematic mean of the dose distribution along with mean dose rates for age estimates. They suggest that since most of the age models require OD inputs in their computation which cannot be determined accurately due to large variation in inherent distribution it is not appropriate to use such models for age estimations. However, as it is known that partial bleaching is also an important component which is present in naturally bleached samples and ignoring it by just considering ratio of arthematic mean dose and sediment dose rate may lead to erroneous result. In such cases the methodology suggested by present work not only takes care of beta heterogeneity but it also minimizes the effect of partially bleached grains. Thus, we with reason, suggest that the use of minimum palaeodose and minimum dose rate is logically the most appropriate way to compute the ages. The error in age can be estimated by propagating the errors of D_e and $\overline{\dot{D}}$, in Eq. (19). δ being a theoretically calculated value is not included in error propagation and can be calculated from Eqs. (20), (21) and (22).

The concordance of results with this prescription with control ages confirms that the approach is robust.

Future possibilities

Present simulation used an identical size (200 µm) of quartz and feldspar grains. In more realistic cases a simulation for variable size grains will be required. The use of variable size grains would affect the results in two ways. In first case it will change the density of matrix due to presence of grains in interstitial and which in turn will change the range of the ^{40}K in the matrix. However, such a case can be represented well by a matrix having density in between solid quartz matrix and a porous matrix simulated in present work.

The second effect can be due to change in sizes of feldspar grains in matrix. This will be a very complex physical situation as different types of sediment matrices will have different distribution in grain sizes and the dose distribution will depend on the distribution of grain sizes and the distribution of K in these. Thus, if K resides in a smaller grain size the heterogeneity of beta dose will diminish and this will accentuate if K is mostly in higher grain size fraction.

Variable grain size approach was adopted by Guérin et al. (2015) but a difference observed from calculations by Mayya et al. (2006). The authors attributed the discrepancies to the simplistic approach followed by Mayya et al. (2006) and also mentioned that it is difficult to compare the two as both the approaches are significantly different. The present work improvises upon the analytical approach suggested by Mayya et al. (2006) and is able to obtain results consistent with independent age estimates. Thus, it is important to develop analytical model further for variable grain sizes.

Conclusion

The present work leads to the following conclusions.

1. The dose deposition function calculated using Monte-Carlo simulations suggests a higher value of the δ as compared to Mayya et al. (2006).The dose deposited at intermediate distances (~ 0.6–2 mm) is higher.
2. Porosity has considerable effect on the δ values when K concentration is low, but at higher concentrations the δ values are almost the same. Thus in respect of heterogeneous distribution of beta dose, at lower concentrations of K, the porosity should be taken in consideration for computation of δ.
3. The ages computed using the beta dose heterogeneity and the equation of Mayya et al. (2006),gave results consistent with published and independent age control (22 out of 24 ages) and therefore methodology is recommended for use in the case of single grain dating.

Supplementary Information The online version contains supplementary material available at https://doi.org/10.1007/s43538-021-00057-y.

Acknowledgements AKS thanks the SERB, Department of Science and Technology, India for the grant of a JC Bose fellowship and Year of Science Chair Professorship and, the Department of Atomic Energy for Raja Ramanna Fellowship. We would also like to thank anonymous reviewers for their constructive comments, which helped significant improvement of the manuscript

References

Adamiec, G., Aitken, M.J.: Dose-rate conversion factors: update. Ancient TL **16**, 37–50 (1998)
Ankjærgaard, C., Murray, A.S.: Total beta and gamma dose rates in trapped charge dating based on beta counting. Radiat. Meas. **42**, 352–359 (2007)
Bateman, M.D., Frederick, C.D., Jaiswal, M.K., Singhvi, A.K.: Investigations into the potential effects of pedoturbation on luminescence dating. Quat. Sci. Rev. **22**, 1169–1176 (2003)
Bateman, M.D., Boulter, C.H., Carr, A.S., Frederick, C.D., Peter, D., Wilder, M.: Detecting post-depositional sediment disturbance in sandy deposits using optical luminescence. Quat. Geochronol. **2**, 57–64 (2007)
Chauhan, N.: Spatial distribution of environmental dose for luminescence dosimetry: Theoretical estimation and applications. Physics Department, Ahmedabad (2011)
Chauhan, N.: Luminescence dating: basic approach to geochronology. Defect Diffus Forum **347**, 111–137 (2014)
Chauhan, N., Morthekai, P.: Chronology of desert margin in western india using improved luminescence dating protocols. J. Earth Syst. Sci. **126**, 115 (2017)
Chauhan, N., Singhvi, A.K.: Distribution in sar palaeodoses due to spatial heterogeniety of natural beta dose. Geochronometria **38**, 190 (2011)
Chauhan, N., Singhvi, A.K.: Changes in the optically stimulated luminescence (osl) sensitivity of single grains of quartz during the measurement of natural osl: implications for the reliability of optical ages. Quat. Geochronol. (2019). https://doi.org/10.1016/j.quageo.2019.101004
Chauhan, N., Anand, S., Palani Selvam, T., Mayya, Y.S., Singhvi, A.K.: Extending the maximum age achievable in the luminescence dating of sediments using large quartz grains: a feasibility study. Radiat. Meas. **44**, 629–633 (2009)
Cunningham, A.C., Devries, D.J., Schaart, D.R.: Experimental and computational simulation of beta-dose heterogeneity in sediment. Radiat. Meas. **47**, 1060–1067 (2012)
Feathers, J.K.: Single-grain osl dating of sediments from the southern high plains. USA. Quat. Sci. Rev. **22**, 1035–1042 (2003). https://doi.org/10.1016/S0277-3791(03)00049-0
Feathers, J.K., Holliday, V.T., Meltzer, D.J.: Optically stimulated luminescence dating of southern high plains archaeological sites. J. Archaeol. Sci. **33**, 1651–1665 (2006a)
Feathers, J.K., Rhodes, E.J., Huot, S., McAvoy, J.M.: Luminescence dating of sand deposits related to late pleistocene human

occupation at the cactus hill site, Virginia, USA. Quat. Geochronol. **1**, 167–187 (2006b)
Galbraith, R.F., Roberts, R.G., Laslett, G., Yoshida, H., Olley, J.M.: Optical dating of single and multiple grains of quartz from jinmium rock shelter, northern australia: Part i. Experimental design and statistical models. Archaeometry **41**, 339–364 (1999)
Guérin, G., Jain, M., Thomsen, K.J., Murray, A.S., Mercier, N.: Modelling dose rate to single grains of quartz in well-sorted sand samples: the dispersion arising from the presence of potassium feldspars and implications for single grain osl dating. Quat. Geochronol. **27**, 52–65 (2015). https://doi.org/10.1016/j.quageo.2014.12.006
Guérin, G., Mercier, N., Nathan, R., Adamiec, G., Lefrais, Y.: On the use of the infinite matrix assumption and associated concepts: a critical review. Radiat. Meas. **47**, 778–785 (2012). https://doi.org/10.1016/j.radmeas.2012.04.004
Jain, M., Murray, A.S., Bøtter-Jensen, L.: Optically stimulated luminescence dating: How significant is incomplete light exposure in fluvial environments? Quaternaire **15**, 143–157 (2004a)
Jain, M., Thomsen, K.J., Bøtter-Jensen, L., Murray, A.S.: Thermal transfer and apparent-dose distributions in poorly bleached mortar samples: results from single grains and small aliquots of quartz. Radiat. Meas. **38**, 101–109 (2004b)
Kawrakow, I., Rogers, D.W.O.: The Egsnrc Code System: Monte Carlo Simulation of Electron and Photon Transport. National Research Council of Canada, Ottawa (2000)
Kelly, W.H., Beard, G.B., Peters, R.A.: The beta decay of k40. Nucl. Phys. **11**, 492–498 (1959)
Mayya, Y.S., Morthekai, P., Murari, M.K., Singhvi, A.K.: Towards quantifying beta microdosimetric effects in single-grain quartz dose distribution. Radiat. Meas. **41**, 1032–1039 (2006)
Murray, A.S., Roberts, R.G.: Determining the burial time of single grains of quartz using optically stimulated luminescence. Earth Plan. Sci. Lett. **152**, 163–180 (1997)
Nathan, R.P., Thomas, P.J., Jain, M., Murray, A.S., Rhodes, E.J.: Environmental dose rate heterogeneity of beta radiation and its implications for luminescence dating: Monte Carlo modelling and experimental validation. Radiat. Meas. **37**, 305–313 (2003)
Olley, J., Caitcheon, G., Murray, A.: The distribution of apparent dose as determined by optically stimulated luminescence in small aliquots of fluvial quartz: implications for dating young sediments. Quat. Sci. Rev. **17**, 1033–1040 (1998)
Olley, J.M., Caitcheon, G.G., Roberts, R.G.: Origin of dose distributions in fluvial sediments, and the prospect of dating single grains from fluvial deposits using optically stimulated luminescence. Radiat. Meas. **30**, 207–217 (1999)
Rogers, D.W.O., Kawrakow, I., Seuntjens, J.P., Walters, B.R.B., Mainegra-Hing, E.: Nrc User Codes for egsnrc PIRS-702. National Research Council of Canada, Ottawa (2005)
Singhvi, A., Stokes, S., Chauhan, N., Nagar, Y., Jaiswal, M.: Changes in natural osl sensitivity during single aliquot regeneration procedure and their implications for equivalent dose determination. Geochronometria **38**, 231–241 (2011). https://doi.org/10.2478/s13386-011-0028-3
Singhvi, A.K., Chauhan, N., Biswas, R.H.: A survey of some new approaches in maximum age limit and accuracy of luminescence application to archaeological chronometry. Mediter. Archaeol. Archaeom. **10**, 9–15 (2010)
Vandenberghe, D., Hossain, S.M., De Corte, F., Van den haute P,: Investigations on the origin of the equivalent dose distribution in a dutch coversand. Radiat. Meas. **37**, 433–439 (2003)